This article has been accepted for publication in a future issue of this journal, but has not been fully edited. Content may change prior to final publication. Citation information: DOI 10.1109/TPAMI.2018.2840719, IEEE Transactions on Pattern Analysis and Machine Intelligence

Distributed Very Large Scale Bundle Adjustment by Global Camera Consensus

Runze Zhang, Siyu Zhu, Tianwei Shen, Lei Zhou, Zixin Luo, Tian Fang and Long Quan *Fellow, IEEE*

Abstract—The increasing scale of Structure-from-Motion is fundamentally limited by the conventional optimization framework for the all-in-one global bundle adjustment. In this paper, we propose a distributed approach to coping with this global bundle adjustment for very large scale Structure-from-Motion computation. First, we derive the distributed formulation from the classical optimization algorithm ADMM, Alternating Direction Method of Multipliers, based on the global camera consensus. Then, we analyze the conditions under which the convergence of this distributed optimization would be guaranteed. In particular, we adopt over-relaxation and self-adaption schemes to improve the convergence rate. After that, we propose to split the large scale camera-point visibility graph in order to reduce the communication overheads of the distributed computing. The experiments on both public large scale SfM data-sets and our very large scale aerial photo sets demonstrate that the proposed distributed method clearly outperforms the state-of-the-art method in efficiency and accuracy.

Index Terms—Bundle Adjustment, Structure-from-Motion, 3D Reconstruction, Distributed Computing

1 Introduction

With the popularization of smartphones and unmanned aerial vehicles, larger collection of images with high quality and resolution are available, which gives rise to dramatic increment of the scale of image-based 3D reconstruction. High quality 3D models obtained from the large-scale high resolution images are beneficial to the digital earth, virtual reality and intelligent city. However, current image-based 3D reconstruction systems still have problems when dealing with large-scale data-sets.

Structure-from-Motion(SfM) is one of core steps in image-based 3D reconstruction. In this step, images are matched, then camera poses and scene structures are reconstructed. The common SfM pipeline includes image matching, relative pose computation, camera registration and the global bundle adjustment. The camera registration step generates initial camera poses in a global coordinate system from camera relative poses, then the global bundle adjustment optimizes all the camera poses and sparse 3D points to obtain high quality results for the following 3D reconstruction steps.

However, the commonly used optimization method in the global bundle adjustment requires all the camera poses and points are stored in the memory. The space cost of bundle adjustment is proportional to the square of the camera number. If there are too many cameras, it is impossible to complete the global bundle adjustment in one machine. Therefore, referring to space division based methods [1], [2] and applying ADMM algorithm [3] to the bundle adjustment problem, we propose an improved consensus framework by camera consensus and splitting points to perform the global bundle adjustment in a distributed manner to solve the scalability problem. In summary, our contributions primarily are as follows:

1) We propose a general consensus framework regardless of the number of parameters of camera and take consideration of the common intrinsic parameters;
2) We analyze the conditions of convergence in detail and adopt the over-relaxation and self-adaption scheme to improve the convergence rate;
3) We propose a splitting method to minimize the overhead in the distributed system.

There are two reasons why ADMM algorithm can be applied to the bundle adjustment problem. One is that the global bundle adjustment is the final step in Structure-from-Motion, so we have a good enough initialization of camera poses obtained by previous steps. The other is that the topological structure of the problem, namely the bipartite camera-point visibility graph, facilitates the division of the large-scale problem.

1.1 Related work

Many works try to tackle city-level and even world level Structure-from-Motion by image sequences or unordered image sets. The work [4] iteratively performs feature detection, relative pose computation and incremental camera registration to generate quasi-dense SfM results. But it requires heavy computation for large-scale and high resolution images. The work [5] adopts an incremental strategy to register cameras. However, with the number of registered cameras growing, the method will be slower. The work [6] resamples the sparse points obtained by Structure-from-Motion to reduce computation cost. Agarwal et al. [7] propose a distributed method to match images and register cameras. To accelerate the registration, they adopt the skeletal set method [8] to register camera hierarchically. Frahm et al. [9] try to implement the method without a distributed system. Then the work [10] reconstructs camera poses from world-wide captured internet images by a stream framework in a single machine. Klingner et al. [11]

- *Runze Zhang, Tianwei Shen, Lei Zhou, Zixin luo and Long Quan are with the Department of Computer Science and Engineering, The Hong Kong University of Science and Technology, Hong Kong SAR.*
  E-mail: {rzhangaj, tshenaa, lzhouai, zluoag, quan}@cse.ust.hk
- *Siyu Zhu is with Alibaba A.I. Labs.*
  E-mail: siting.zsy@alibaba-inc.com
- *Tian Fang is with Shenzhen Zhuke Innovation Technology.*
  E-mail: fangtian@altizure.com

This article has been accepted for publication in a future issue of this journal, but has not been fully edited. Content may change prior to final publication. Citation information: DOI 10.1109/TPAMI.2018.2840719, IEEE Transactions on Pattern Analysis and Machine Intelligence

try to deal with the large-scale street-view SfM problem while handling moving rolling shutter cameras. Schonberger et al. [12] propose a new method to register one camera to a large-scale SfM system and recover the lost details. The work [13] proposes a newly graph based image matching method to solve the ambiguity problem of large-scale SfM, and the work [14] proposes a new SfM technique to improve the robustness, accuracy, completeness and scalability. However, these works do not pay attention to the global optimization of camera poses in the end of SfM. Since the global optimization called bundle adjustment has too large scale cost to be completed by limited memory and time, it is difficult to perform for large scale data-sets.

The bundle adjustment is the non-linear optimization to refine the camera parameters and 3D points in the end of Structure-from-Motion. The Levenberg-Marquardt algorithm [15] with Schur complement is the most common method to optimize the bundle adjustment formulation, which takes advantages of the sparsity in the multiple-view geometry problem. The work [16] tries to improve the efficiency of the large scale bundle adjustment problem by factorization and precondition method, and [17] proposes a method to group factors for the bundle adjustment problem. The preconditioner based on the camera visibility graph is also adopted in work [18], [19] to improve the efficiency of LM algorithm. The work [20] implements the optimization algorithm of bundle adjustment in parallel for acceleration by improving the CPU utilization. However, those methods are still single-machine methods which cannot solve the problem with too large scale to be loaded into memory.

Some works try to tackle the large scale bundle adjustment problem by out-of-core algorithms [21], [22] and the distributed system [23] to break through the memory limitation of the single-machine algorithm. The out-of-core method [21] splits the large scale bundle adjustment problem into several small problems, solves the small problems in parallel and merges them iteratively by the optimization of overlapping region of those small problems. However, for densely captured data-sets, the splitting will yield too large overlapping regions to be loaded into memory to do optimization. Besides, the I/O overhead induced by overlapping regions is also too high. In the following work [22], the author utilizes a hierarchical framework to split the large problem and merge small problems in each level by the smooth method [24]. Nevertheless, the hierarchical framework sacrifices the degree of parallelism and is difficult to implement in a distributed system. The smooth method to merge small problems cannot guarantee the bundle adjustment result is optimized.

The work in [23] proposes a consensus framework to deal with large scale bundle adjustment in a distributed manner. Instead of merging small problems by the optimization of overlapping regions of small problems, the consensus framework utilizes the proximal splitting method to formulate the bundle adjustment problem, in which the small problems are merged by averaging points in fact, decreasing the cost of merging. The merging process for the same parameters guarantees the consensus of points in different nodes. Thus, we call this method point consensus based distributed bundle adjustment. However, the consensus framework based on point consensus and splitting by cameras in [23] still has some problems in practice. Firstly, in each iteration, each node in the distributed system has to broadcast all overlapping points to the master node to complete the merging process, which is a huge overhead for large scale data-sets. Secondly, parameters of each camera are independent of parameters of other cameras. However, in practice, some cameras may share the same intrinsic parameters. Thirdly, the method by merging points converges a little slowly in very large scale data-sets and may converge in a local minimum early.

The Alternating Direction Method of Multipliers(ADMM) algorithm [3] is a useful tool to solve distributed optimization problems. This algorithm decomposes the original problem into different small sub-problems and then the solutions of those sub-problems are merged to find the global solutions. The topological structure of the bundle adjustment problem is suitable for the decomposition in ADMM algorithm. By our analysis and experiments, the ADMM algorithm can work on the bundle adjustment problem though the bundle adjustment problem cannot satisfy the convex condition required by ADMM algorithm. By adopting ADMM algorithm and performing consensus on cameras, we propose the method to solve the large-scale bundle adjustment problem distributedly.

The rest of the paper is organized as follows. We will first review the bundle adjustment problem and the camera model in section 2.1. Then, we will introduce the ADMM algorithm and the consensus method based on the ADMM in section 2.2. In section 2.3, we derive the iteration equations for camera consensus based distributed bundle adjustment from the ADMM algorithm. After that, we will analyze the conditions to guarantee the convergence in 3.1. The relaxation and self-adaption scheme are introduced in section 3.2 to improve the convergence rate. In section 4, we propose a scalable splitting method to minimize the overhead in the distributed system and describe the implementation detail. Then, we will show the experimental results in section 5, demonstrating that our method can solve the large scale bundle adjustment problem in a distributed system efficiently and accurately. At last, we will discuss some problems in practice and the future work in section 6.

2 The Distributed Formulation

In this section, we will first introduce the bundle adjustment problem and the camera model. Then we will describe the global consensus problem solved by the Alternating Direction Method of Multipliers(ADMM) and then apply the solution to the bundle adjustment problem by camera consensus.

2.1 Bundle adjustment

Generally, camera parameters consist of extrinsic parameters and intrinsic parameters. Extrinsic parameters are independent for different cameras but intrinsic parameters may be shared by different cameras. Suppose we have M observed 3D points, N cameras sharing L different intrinsic parameters, note camera extrinsic parameter set $\mathcal{E} = \{\mathbf{e}_i \in \mathbb{R}^C | i = 1, ..., N\}$, camera intrinsic parameter set $\mathcal{D} = \{\mathbf{d}_l \in \mathbb{R}^I | l = 1, ..., L\}$, observed 3D point set $\mathcal{P} = \{\mathbf{p}_j \in \mathbb{R}^3 | j = 1, ..., M\}$ and detected observation set $\mathcal{Q} = \{\mathbf{q}_{ij} \in \mathbb{R}^2 | \mathbf{p}_j \in \mathcal{V}_i\}$, where $\mathcal{V}_i$ is the set of points viewed by the ith camera. Note that $\mathbf{e}_i$ is not the extrinsic matrix of the ith camera, but the parameterization of extrinsic parameters. The bundle adjustment is a non-linear least square optimization problem to obtain the optimized cameras and 3D points with the following objective function:

$$f(\mathcal{E}, \mathcal{D}, \mathcal{P}) = \sum_{i=1}^{n} \sum_{\mathbf{p}_j \in \mathcal{V}_i} ||\mathbf{\Pi}(\mathbf{e}_i, \mathbf{d}_{l_i}, \mathbf{p}_j) - \mathbf{q}_{ij}||_2^2, \quad (1)$$

This article has been accepted for publication in a future issue of this journal, but has not been fully edited. Content may change prior to final publication. Citation information: DOI 10.1109/TPAMI.2018.2840719, IEEE Transactions on Pattern Analysis and Machine Intelligence

where $\mathbf{d}_{l_i}$ is the intrinsic parameters of the ith camera and $\Pi(\mathbf{e}_i, \mathbf{d}_{l_i}, \mathbf{p}_j)$ computes the reprojection of the jth point in the ith camera, which is non-linear and non-convex. The computation $\Pi(\mathbf{e}_i, \mathbf{d}_{l_i}, \mathbf{p}_j)$ depends on the camera model and we use the pinhole camera model with radial distortion. Here, camera center $\mathbf{c}_i$ and parameterization of rotation $\mathbf{r}_{Ri}$ are used to express the extrinsic parameter of camera $\mathbf{e}_i$, namely $\mathbf{e}_i = (\mathbf{r}_{Ri}, \mathbf{c}_i)$. The parameterization of rotation will be discussed in section 3.1.

The commonly used optimization methods, such as Levenberg-Marquardt algorithm [15] with sparse matrix and Schur complement, have space cost $O(N(N+M))$, which is difficult to optimize large scale data-sets with too many cameras and sparse points.

2.2 The global consensus based on ADMM

The Alternating Direction Method of Multipliers(ADMM) algorithm [3] aims to solve the problem in the form:

$$\begin{aligned} &\text{minimize} && f(\mathbf{x}) + g(\mathbf{z}) \\ &\text{subject to} && \mathbf{A}\mathbf{x} + \mathbf{B}\mathbf{z} = \mathbf{w} \end{aligned} \tag{2}$$

By the augmented Lagrangian multipliers method, we form

$$\begin{aligned} L_\rho(\mathbf{x}, \mathbf{z}, \mathbf{y}) = f(\mathbf{x}) + g(\mathbf{z}) + \mathbf{y}^T(\mathbf{A}\mathbf{x} + \mathbf{B}\mathbf{z} - \mathbf{w}) \\ + \frac{\rho}{2}||\mathbf{A}\mathbf{x} + \mathbf{B}\mathbf{z} - \mathbf{w}||_2^2 \end{aligned} \tag{3}$$

The ADMM algorithm consists of the iterations:

$$\mathbf{x}^{t+1} = \arg\min_{\mathbf{x}} L_\rho(\mathbf{x}, \mathbf{z}^t, \mathbf{y}^t) \tag{4}$$

$$\mathbf{z}^{t+1} = \arg\min_{\mathbf{z}} L_\rho(\mathbf{x}^{t+1}, \mathbf{z}, \mathbf{y}^t) \tag{5}$$

$$\mathbf{y}^{t+1} = \mathbf{y}^t + \rho(\mathbf{A}\mathbf{x}^{t+1} + \mathbf{B}\mathbf{z}^{t+1} - \mathbf{w}) \tag{6}$$

In the implementation, $\mathbf{x}$, $\mathbf{y}$ and $\mathbf{z}$ are updated by an alternating fashion.

Now, we want to solve this global consensus problem:

$$\begin{aligned} &\text{minimize} && \sum_{i=1}^{n} f_i(\mathbf{x}_i) \\ &\text{subject to} && \mathbf{x}_i = \mathbf{z}, i = 1, ..., n \end{aligned} \tag{7}$$

Using ADMM, we can derive the iteration expression as

$$\begin{aligned} \mathbf{x}_i^{t+1} = \arg\min_{\mathbf{x}_i}(f_i(\mathbf{x}_i) + \left(\mathbf{y}_i^t\right)^T(\mathbf{x}_i - \mathbf{z}^t) \\ + \frac{\rho}{2}||\mathbf{x}_i - \mathbf{z}^t||_2^2) \end{aligned} \tag{8}$$

$$\mathbf{z}^{t+1} = \frac{1}{n}\sum_{i=1}^{n}\mathbf{x}_i^{t+1} \tag{9}$$

$$\mathbf{y}_i^{t+1} = \mathbf{y}_i^t + \rho(\mathbf{x}_i^{t+1} - \mathbf{z}^{t+1}), i = 1, ..., n \tag{10}$$

Substituting $\mathbf{y}_i = \rho\mathbf{u}_i$, we can express equations 8 and 10 as

$$\mathbf{x}_i^{t+1} = \arg\min_{\mathbf{x}_i} f_i(\mathbf{x}_i) + \frac{\rho}{2}\left\|\mathbf{x}_i - (\mathbf{z}^t - \mathbf{u}_i^t)\right\|_2^2 \tag{11}$$

$$\mathbf{u}_i^{t+1} = \mathbf{u}_i^t + \mathbf{x}_i^{t+1} - \mathbf{z}^{t+1}, \tag{12}$$

Defining the proximity operator $\mathbf{prox}_{f/\rho}$ of one function $f(x)$ with $\rho > 0$ as $\mathbf{prox}_{f/\rho}(a) = f(x) + \frac{\rho}{2}\|x - a\|_2^2$, we can express the right of Eqn. 11 as $\mathbf{prox}_{f_i/\rho}(\mathbf{z}^t - \mathbf{u}_i^t)$. The computation of equations 11 and 12 can be performed easily in a distributed system. Eqn. 9 actually averages the results of optimization results in different nodes.

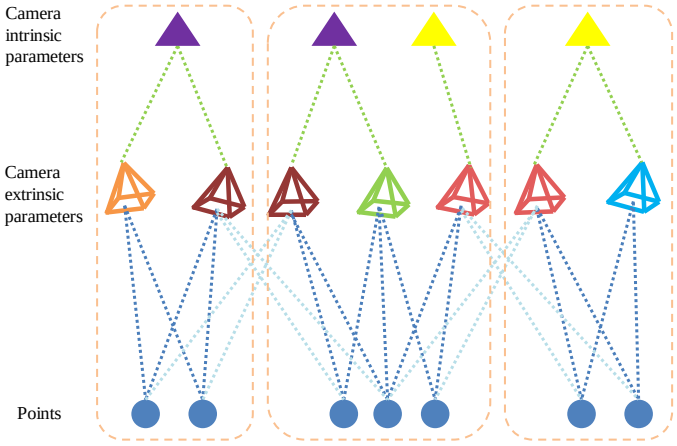

Fig. 1: The camera extrinsic and intrinsic parameters with the same color are the component of the same parameter in different blocks. The links between cameras and points with the light color are the lost links due to the splitting.

2.3 Camera Consensus

Actually, the iterations of equations 8, 9, and 10 are indeed the Douglas-Rachford splitting method in [23]. By clarifying the derivation of the method, we can explain the stop criterion, over-relaxation and self-adaption scheme in section 3. The work [23] performs the consensus framework based on points. However, very large scale data-sets always contain so many points that the distributed system has huge overhead to broadcast those points. Besides, intuitively, the averaging of too many variables in Eqn. 9 leads to slow convergence rate. Hence, we try to reduce the overhead of broadcasting of $\mathbf{x}_i$ and $\mathbf{y}_i$ in the averaging for very large scale bundle adjustment problem by camera consensus instead of points.

In order to broadcast cameras instead of points in [23], we split the whole bundle adjustment problem by points. Note each block as $\mathcal{B}_k = (\mathcal{E}_k, \mathcal{D}_k, \mathcal{P}_k), k = 1, ..., K$, where $\mathcal{P}_k$ is the set of points in the block so that $\mathcal{P}_{k_1} \cap \mathcal{P}_{k_2} = \phi$ and $\bigcup \mathcal{P}_k = \mathcal{P}$. Since one camera may view points in different block, extrinsic parameters of one camera can appear in different block. We define $\mathbf{e}_i^k$ as the extrinsic parameter of the ith camera in block k and $\mathcal{E}_k = \{\mathbf{e}_i^k | \text{the } i\text{th camera views points in the } k\text{th block}\}$. Similar to extrinsic parameters, one intrinsic parameter may be shared by cameras in different blocks, so we define $\mathbf{d}_l^k$ as the lth intrinsic parameter in the kth block and $\mathcal{D}_k = \{\mathbf{d}_l^k | \text{the } l\text{th intrinsic parameter is shared by cameras in the } k\text{th block}\}$. Note n_i and m_l are the number of blocks where the ith extrinsic or the lth intrinsic parameter appear. The relationship of those parameters are shown in Fig. 1.

Then, we can modify the original bundle adjustment problem in Eqn. 1 as

$$\begin{aligned} &\text{minimize} && \sum_{k=1}^{K} f(\mathcal{E}_k, \mathcal{D}_k, \mathcal{P}_k) \\ &\text{subject to} && \mathbf{e}_i^k = \mathbf{e}_i, i = 1, ..., N, k = 1, ..., K \\ & && \mathbf{d}_l^k = \mathbf{d}_l, l = 1, ..., L, k = 1, ..., K, \end{aligned} \tag{13}$$

where we force all the camera parameters $\mathbf{e}_i^k$ and $\mathbf{d}_l^k$ which appear in different blocks to be equal to the global variables $\mathbf{e}_i$ and $\mathbf{d}_l$.

This article has been accepted for publication in a future issue of this journal, but has not been fully edited. Content may change prior to final publication. Citation information: DOI 10.1109/TPAMI.2018.2840719, IEEE Transactions on Pattern Analysis and Machine Intelligence

Using the ADMM algorithm, we can obtain the iterations for the above problem:

$$\begin{aligned}(\mathcal{E}_k,\mathcal{D}_k,\mathcal{P}_k)^{t+1} &= \arg\min(f(\mathcal{E}_k,\mathcal{D}_k,\mathcal{P}_k) \\ &\quad + h(\mathcal{E}_k,\mathcal{D}_k,\mathcal{P}_k)),\forall k\end{aligned} \tag{14}$$

$$\mathbf{e}_i^{t+1} = \sum\nolimits_{\mathcal{E}_k \ni \mathbf{e}_i^k} \left(\mathbf{e}_i^k\right)^{t+1} / n_i, \forall i, \qquad \mathbf{d}_l^{t+1} = \sum\nolimits_{\mathcal{D}_k \ni \mathbf{d}_l^k} \left(\mathbf{d}_l^k\right)^{t+1} / m_l, \forall l, \tag{15}$$

$$\left(\widetilde{\mathbf{e}}_i^k\right)^{t+1} = \left(\widetilde{\mathbf{e}}_i^k\right)^{t} + \left(\mathbf{e}_i^k\right)^{t+1} - \mathbf{e}_i^{t+1}, \forall i,k \qquad \left(\widetilde{\mathbf{d}}_l^k\right)^{t+1} = \left(\widetilde{\mathbf{d}}_l^k\right)^{t} + \left(\mathbf{d}_l^k\right)^{t+1} - \mathbf{d}_l^{t+1}, \forall l,k, \tag{16}$$

where $f(\mathcal{E}_k,\mathcal{D}_k,\mathcal{P}_k)$ is the bundle adjustment objective function on variables in the kth block and

$$\begin{aligned}h(\mathcal{E}_k,\mathcal{D}_k,\mathcal{P}_k) &= \frac{1}{2}\sum\nolimits_{\mathbf{e}_i^k\in\mathcal{E}_k}\left\|\mathbf{e}_i^k - \mathbf{e}_i^t + \left(\widetilde{\mathbf{e}}_i^k\right)^t\right\|_{\mathbf{\Sigma}_e}^2 \\ &\quad + \frac{1}{2}\sum\nolimits_{\mathbf{d}_l^k\in\mathcal{D}_k}\left\|\mathbf{d}_l^k - \mathbf{d}_l^t + \left(\widetilde{\mathbf{d}}_l^k\right)^t\right\|_{\mathbf{\Sigma}_d}^2 \\ &\quad + \frac{\rho_p}{2}\sum\nolimits_{\mathbf{p}_j\in\mathcal{P}_k}\left\|\mathbf{p}_j - \mathbf{p}_j^t\right\|_2^2\end{aligned} \tag{17}$$

In Eqn. 17, unlike the method in [23] that the proximity operator does not work on the non-consensus items, the proximity operator here also works on points which do not attend the consensus in Eqn. 9. The reason will be introduced in section 3.1. For the term on camera parameters in Eqn. 17, we use $\|\cdot\|_{\mathbf{\Sigma}_e}$ and $\|\cdot\|_{\mathbf{\Sigma}_d}$ to replace the $l2$ norm, where $\mathbf{\Sigma}_e$ and $\mathbf{\Sigma}_d$ are a diagonal matrix whose diagonal elements are formed by penalty parameters $\boldsymbol{\rho}_e$ and $\boldsymbol{\rho}_d$. Since each parameter has its domain, each parameter should have their own penalty parameters according to its range. In above iterations, equations 14 and 16 can be implemented distributedly and camera parameters have to be broadcasted to complete the computing in Eqn. 15. The distributed bundle adjustment algorithm based on camera consensus is concluded below:

function DBACC($\mathcal{E}$, $\mathcal{P}$, $\mathcal{D}$, $\mathcal{Q}$, K)
  Initialize all $\widetilde{\mathbf{e}}_i^k$ and $\widetilde{\mathbf{d}}_l^k$ as 0
  Initialize all $\mathbf{e}_i^k$ and $\mathbf{d}_l^k$ as the corresponding initial values of $\mathbf{e}_i$ and $\mathbf{d}_l$
  while the criterion in Eqn. 19 is not satisfied **do**
    for each block $k \in [1, K]$ distributedly **do**
      for each $\mathbf{e}_i$ in block k in parallel **do**
        $\widetilde{\mathbf{e}}_i^k \leftarrow \widetilde{\mathbf{e}}_i^k + \mathbf{e}_i^k - \mathbf{e}_i$
      end for
      for each $\mathbf{d}_l$ in block k in parallel **do**
        $\widetilde{\mathbf{d}}_l^k \leftarrow \widetilde{\mathbf{d}}_l^k + \mathbf{d}_l^k - \mathbf{d}_l$
      end for
      $(\mathcal{E}_k,\mathcal{D}_k,\mathcal{P}_k) \leftarrow \arg\min f(\mathcal{E}_k,\mathcal{D}_k,\mathcal{P}_k) + h(\mathcal{E}_k,\mathcal{D}_k,\mathcal{P}_k)$
    end for
    Broadcast $\mathcal{E}_k$ and $\mathcal{D}_k$ of all nodes to the master node
    Average $\mathcal{E}_k$ and $\mathcal{D}_k$ in the master node by Eqn. 15 to get $\mathcal{E}$ and $\mathcal{D}$
  end while
end function

2.3.1 Stopping criterion

Referring to [25], we define the primal residual $\mathbf{r}^t$ and the dual residual $\mathbf{s}^t$ as

$$\begin{aligned}\|\mathbf{r}^t\|_2^2 &= \sum\left\|\left(\mathbf{e}_i^k\right)^t - \mathbf{e}_i^t\right\|_2^2 + \sum\left\|\left(\mathbf{d}_l^k\right)^t - \mathbf{d}_l^t\right\|_2^2 \\ \|\mathbf{s}^t\|_2^2 &= \sum\|\mathbf{e}_i^{t+1} - \mathbf{e}_i^t\|_{\mathbf{\Sigma}_e}^2 + \sum\|\mathbf{d}_l^{t+1} - \mathbf{d}_l^t\|_{\mathbf{\Sigma}_d}^2 \\ &\quad + \rho_p^2\sum\left\|\mathbf{p}_j^{t+1} - \mathbf{p}_j^t\right\|_2^2\end{aligned} \tag{18}$$

Then, the stopping criterion is that $l2$ norms of the primal residual and dual residual are less than their thresholds

$$\left\|\mathbf{r}^t\right\|_2 < \epsilon^{pri}, \left\|\mathbf{s}^t\right\|_2 < \epsilon^{dual} \tag{19}$$

3 Convergence of Camera Consensus

In this section, we will first analyze the convergence conditions for the proposed algorithm. Then, we will discuss on some extensions to accelerate the algorithm.

3.1 Convergence conditions

ADMM algorithm requires that the function $f_i(x)$ in Eqn. 7 should be convex. However, the bundle adjustment objective function in Eqn. 1 is non-convex. Some works such as [26], [27], [28], [29], [30], [31] analyze the proximal splitting method on non-convex problems and the work [23] proposes a statement for the convergence of Douglas-Rachford splitting applied to the bundle adjustment problem with point consensus. The latest work [30] on ADMM for non-convex problems proposes the gradient Lipschitz-continuity condition, which is similar with our following analysis.

In the following, we will analyze the convergence conditions of the proposed method and provide the provable statement for the convergence. The convergence proof is provided in the supplementary material.

In the convergence proof of ADMM on convex functions in [25], the proof depends on the convexity of $L_\rho(\mathbf{x},\mathbf{z}^t,\mathbf{y}^t)$ in Eqn. 4 guaranteed by the convexity of $f(\mathbf{x})$, so that $\mathbf{x}^{t+1}$ minimizes it. If $f(\mathbf{x})$ is not convex, according to the propositions and theorems in [27], we can let $\nabla f(\mathbf{x})$ be local Lipschitz-continuous to guarantee $L_\rho(\mathbf{x},\mathbf{z}^t,\mathbf{y}^t)$ be local convex when $\rho > \rho_{min}$. Considering each sub-problem $f_i(\mathbf{x})$ in the global consensus problem in Eqn. 7, whose gradient is local Lipschitz-continuous with Lipschitz constant λ_i, let

$$\Psi_i(\mathbf{x}) = f_i(\mathbf{x}_i) + \frac{\rho}{2}\|\mathbf{x}_i - \mathbf{a}\|_2^2, \tag{20}$$

where $\mathbf{a} = \mathbf{z}^t - \mathbf{u}_i^t$. Namely, $\Psi_i(\mathbf{x})$ is the objective function in Eqn. 11, another form of $L_\rho(\mathbf{x},\mathbf{z}^t,\mathbf{y}^t)$. Then $\forall\mathbf{b},\mathbf{c}\in\mathbb{R}^n$, we have

$$\begin{aligned}&(\nabla\Psi_i(\mathbf{b}) - \nabla\Psi_i(\mathbf{c}))^T(\mathbf{b}-\mathbf{c}) \\ =&(\nabla f_i(\mathbf{b}) - \nabla f_i(\mathbf{c}))^T(\mathbf{b}-\mathbf{c}) + \rho\|\mathbf{b}-\mathbf{c}\|_2^2 \\ \geq&(\rho-\lambda_i)\|\mathbf{b}-\mathbf{c}\|_2^2,\end{aligned} \tag{21}$$

Therefore, if we select ρ such that it is larger than $\max\{\lambda_i\}$, $\Psi_i(\mathbf{x})$ is local convex. Since the Lipschitz-continuity is defined on all variables in above analysis, the proximity operator should work on all variables in Eqn. 17, though points do not participate in the consensus. Based on the Lipschitz-continuity requirement, we then check the objective function of bundle adjustment.

This article has been accepted for publication in a future issue of this journal, but has not been fully edited. Content may change prior to final publication. Citation information: DOI 10.1109/TPAMI.2018.2840719, IEEE Transactions on Pattern Analysis and Machine Intelligence

To make the analysis easier, we first consider the reprojection function of pinpole camera without distortions. Note the intrinsic matrix of the camera as $\mathbf{K}$ and the camera matrix $\mathbf{C} = [\mathbf{M}|\mathbf{m}] = \mathbf{K}\mathbf{R}[\mathbf{I}|-\mathbf{c}]$. Then the reprojection funtion in Eqn. 1 $\Pi(\mathbf{e},\mathbf{d},\mathbf{p}) = [(\mathbf{M}_1\mathbf{p}+m_1)/(\mathbf{M}_3\mathbf{p}+m_3), (\mathbf{M}_2\mathbf{p}+m_2)/(\mathbf{M}_3\mathbf{p}+m_3)]$, where $\mathbf{M}_i$ is the ith row of $\mathbf{M}$ and m_i is the ith element of $\mathbf{m}$. Then the error function of each reprojection $\epsilon(\mathbf{e},\mathbf{d},\mathbf{p}) = (\alpha^2+\beta^2)/\gamma^2$ in Eqn. 1, where

$$\begin{bmatrix} \alpha \\ \beta \\ \gamma \end{bmatrix} = \begin{bmatrix} \mathbf{M}_1\mathbf{p} + m_1 - q\left(\mathbf{M}_3\mathbf{p} + m_3\right) \\ \mathbf{M}_2\mathbf{p} + m_2 - q\left(\mathbf{M}_3\mathbf{p} + m_3\right) \\ \mathbf{M}_3\mathbf{p} + m_3 \end{bmatrix}. \tag{22}$$

Since above expression is linear in $\mathbf{p}$ and $\mathbf{C}$ respectively, we can write $[\alpha,\beta,\gamma]^T = A_{\mathbf{p}}\overrightarrow{\mathbf{C}} = A_{\mathbf{C}}\mathbf{p} + a_{\mathbf{C}}$, where $\overrightarrow{\mathbf{C}}$ is the vector formed by terms in $\mathbf{C}$. Then, according to [32],

$$\frac{\partial\epsilon}{\partial\mathbf{C}} = \frac{2}{\gamma^2}A_{\mathbf{p}}^T[\alpha,\beta,-\frac{\alpha^2+\beta^2}{\gamma}]^T \tag{23}$$

$$\frac{\partial\epsilon}{\partial\mathbf{p}} = \frac{2}{\gamma^2}A_{\mathbf{C}}^T[\alpha,\beta,-\frac{\alpha^2+\beta^2}{\gamma}]^T \tag{24}$$

The above gradients have a divisor γ which break the lipschitz-continuity. To avoid the situation where $\gamma \to 0$, we must assume $\gamma \geq d_{min} > 0$, namely depths of any points in any cameras are larger than d_{min}. By this way, the lipschitz constant λ_i in Eqn 21 is bounded. However, this assumption makes the variable domain non-convex. Note Ω as the domain of variables that make depths are less than d_{min}. Since d_{min} can be set small, Ω is also small. We have to guarantee that the variables are not in Ω in the optimization process. This is indeed uneasy for general non-convex optimization problem. Fortunately, the global bundle adjustment problem has a good initialization from previous SfM steps and the depths of scenes to be reconstructed are usually larger than a small d_{min}. This two conditions guarantee that the initial and the optimal variables are neither in Ω. Besides, the good initialization enables us to assume the initial and optimal variables are close, so we can assume any variable values in the iteration should not be in Ω.

Then we will analyze $\partial\epsilon/\partial\mathbf{x} = \partial\epsilon/\partial\mathbf{C}\cdot\partial\mathbf{C}/\partial\mathbf{x}$, where $\mathbf{x}$ can be camera rotations, centers, focal length or principle point. It is clear that $\mathbf{C}$ is linear with camera center, focal length and principle point, so the partial differential of ϵ on them will not break the lipschitz-continuity. However, the partial differential on rotation may have problems. We need consider the parameterization of rotation. Note the parameterization of rotation $\mathbf{R}$ as $\mathbf{r}_R$. Then $\partial\mathbf{C}/\partial\mathbf{r}_R = \partial\mathbf{C}/\partial\mathbf{R}\cdot\partial\mathbf{R}/\partial\mathbf{r}_R$. $\partial\mathbf{C}/\partial\mathbf{R}$ should be constant with $\mathbf{R}$, so we must guarantee $\partial\mathbf{R}/\partial\mathbf{r}_R$ be local Lipschitz-continuous. The commonly used parameterization of rotation includes quaternion and angle-axis($\mathbf{v} = \theta\mathbf{w} \in \mathbb{R}^3$). The map of quaternion to rotation matrix involves the normalization of quaternion, so the gradient is unbounded when quaternion approaches zero. Besides, quaternion is an over-parameterization for rotation, so it leads to communication redundancy. If we use angle-axis as the parameterization of rotations, according to [33],

$$\frac{\partial\mathbf{R}}{\partial v_i} = \frac{v_i\left[\mathbf{v}\right]_\times + \left[\mathbf{v}\times(\mathbf{I}-\mathbf{R})\mathbf{I}_i\right]_\times}{\left\|\mathbf{v}\right\|^2}\mathbf{R}, \tag{25}$$

where $\mathbf{I}_i$ is the ith row of identity matrix $\mathbf{I}$. Although $\|\mathbf{v}\|^2$ is the divisor here, [33] shows $\lim_{\mathbf{v}\to\mathbf{0}}\partial\mathbf{R}/\partial v_i = [\mathbf{I}_i]_\times$, which is a constant. Therefore, the gradient of the exponential map can be proved as Lipschitz-continuous and angle-axis is the minimum description for rotation. Hence, angle-axis can be adopted as the parameterization of rotation in the proposed algorithm.

If the camera model contains distortions, the commonly used radial distortion does not involve any division or square root, so it will not induce other elements to break local Lipschitz-continuity.

Based on above analysis, we can conclude the following statement.

Theorem 1. *With the bundle adjustment objective function 1, let $\{\mathcal{E}^t,\mathcal{D}^t,\mathcal{P}^t\} \subset \mathbb{R}^{6N}\times\mathbb{R}^{IL}\times\mathbb{P}^{3M}$ denote a sequence generated by Algorithm 1, where I is the dimension of intrinsic parameter and each $\mathcal{E}^t = \{(\mathbf{r}_R^t,\mathbf{c}^t)\} \in \mathbb{R}^{3N}\times\mathbb{R}^{3N}$ where $\mathbf{r}_R$ is the angle-axis presentation of rotation and $\mathbf{c}$ is the camera center. Suppose the gradient of distortion function is Lipschitz-continuous and the scene depth d is bounded from below by $\mathbf{M}_{i3}^T\mathbf{p}_j + m_{i3} \geq d_{min} > 0$ for all cameras and points in the sequence generated by Algorithm 1, then, there exists a $\boldsymbol{\rho}_{min} = (\boldsymbol{\rho}_e^{min},\boldsymbol{\rho}_d^{min},\rho_p^{min})$ such that if each element in $\boldsymbol{\rho}$ of Algorithm 1 is larger than the corresponding one in $\boldsymbol{\rho}_{min}$, Algorithm 1 is guaranteed to converge to a local minimum of Eqn. 1.*

There are four differences of the statement from the one in [23]. Firstly, the rotation parameterization is required as angle-axis to satisfy the local Lipschitz-continuity since the proximity operator works on camera parameters. Secondly, we consider distortions of the camera model and give the requirement of distortion function. Thirdly, we also consider the non-consensus term and its penalty to guarantee the local Lipschitz-continuity more validly. Lastly, the depth conditions are more strong that requires all the depths computed by variables in the sequence should larger than d_{min}. This is still an acceptable condition for a good initialization from previous SfM steps. We will discuss the situation this condition is not satisfied in section 6.3.

3.2 Improving convergence rate

In this section, we will introduce two extensions of ADMM algorithm to improve the convergence rate.

3.2.1 Self-adaption penalty

It is obvious that if the penalty parameter $\boldsymbol{\rho}$ is too large, the algorithm will converge slowly. Otherwise, the algorithm will yield diverged results according to the analysis in section 3.1. According to the iterations in Eqn. 17, large penalty on violations of primal feasibility results in small primal residual $\mathbf{r}$. Conversely, small penalty leads to small dual residual according to the definition of dual residual $\mathbf{s}$ in Eqn. 18. Therefore, we adopt the scheme introduced in [34].

$$\rho_x^{t+1} = \begin{cases} \tau^{incr}\rho_x^t & \text{if} \|\mathbf{r}_x^t\|_2 > \mu_1\|\mathbf{s}_x^t\|_2 \\ \rho_x^t/\tau^{decr} & \text{if} \|\mathbf{s}_x^t\|_2 > \mu_2\|\mathbf{r}_x^t\|_2 \\ \rho_x^t & \text{otherwise} \end{cases} \tag{26}$$

where ρ_x, $\mathbf{s}_x$ and $\mathbf{r}_x$ mean the different components of $\boldsymbol{\rho}$, $\mathbf{s}$ and $\mathbf{r}$ corresponding to the parameters of different cameras. Since each parameter is independent, we adopt different penalty parameters for different parameters of different cameras and points. Since $\mathbf{u}_i = \mathbf{y}_i/\rho$ in Eqn. 12, when ρ multiplies τ, the corresponding $\widetilde{\mathbf{e}}_k^t$ and $\widetilde{\mathbf{d}}_k^t$ should be divided by τ.

This article has been accepted for publication in a future issue of this journal, but has not been fully edited. Content may change prior to final publication. Citation information: DOI 10.1109/TPAMI.2018.2840719, IEEE Transactions on Pattern Analysis and Machine Intelligence

3.2.2 Over-relaxation

Over-relaxation scheme can be adopted in the ADMM iteration of Eqn. 6 according to the analysis in [35], where $\mathbf{A}\mathbf{x}^{t+1}$ can be replaced with $(1+\alpha^t)\mathbf{A}\mathbf{x}^{t+1} + \alpha^t(\mathbf{B}\mathbf{z}^t - \mathbf{w})$ in the iteration of Eqn. 6. Substituting the bundle adjustment configuration to the over-relaxation scheme, we can obtain the over-relaxed iteration of Eqn. 16:

$$\begin{aligned}\left(\widetilde{\mathbf{e}}_i^k\right)^{t+1} &= \left(\widetilde{\mathbf{e}}_i^k\right)^{t} + (1+\alpha^t)\left(\left(\mathbf{e}_i^k\right)^{t+1} - \mathbf{e}_i^{t+1}\right), \forall i,k \\ \left(\widetilde{\mathbf{d}}_l^k\right)^{t+1} &= \left(\widetilde{\mathbf{d}}_l^k\right)^{t} + (1+\alpha^t)\left(\left(\mathbf{d}_l^k\right)^{t+1} - \mathbf{d}_l^{t+1}\right), \forall l,k,\end{aligned} \tag{27}$$

where $\alpha^t \in (0,1]$ and $\lim_{t\to\infty}\sum \alpha^t(1-\alpha^t) = +\infty$ [36]. The experiments in [37], [38] suggest that $\alpha^t \in [0.5, 0.8]$ should improve the convergence rate.

4 The Distributed Implementation

In this section, we will describe the implementation details to reduce the overhead further more and improve the convergence rate.

4.1 Block splitting

Few previous works on the parallel or distributed bundle adjustment discuss how to split blocks. [21] adopts graph cut to get a partition minimizing the edges that span the visibility graph, so that the overlapped region including cameras and points is minimized. Our method only broadcasts all the cameras in different nodes to the master node to compute Eqn. 15. Suppose parameters of each camera are independent, the total overhead of one iteration in our distributed method is proportional to

$$\sum\nolimits_{i=1}^{K} |\mathcal{E}_k| = \sum\nolimits_{i=1}^{N} n_i, \tag{28}$$

However, it is NP-hard to minimize the above overhead. Referring to [21], we transform the problem to a graph cut problem on the camera-point visibility graph.

If the ith camera appears in n_i blocks, the number of links between the camera and its visible points which will be cut (the link with the light color shown in Fig.1) is at least $n_i - 1$. Hence, $\sum_{i=1}^{N} n_i \leq \sum_{i=1}^{N} E_i + n$, where E_i is the number of cut edges on the ith camera. Therefore, we can minimize the upper bound of Eqn. 28 by graph-cut in the visibility graph between cameras and points to obtain the sub-optimization of Eqn. 28. Meanwhile, it is better that each block has unbiased number of cameras and points to balance the load of each node. Therefore, Normalized-Cut [39] is a proper algorithm to implement the graph cut. After the graph cut, we collect points and cameras viewing those points in different blocks.

However, for very large scale data-sets with high capturing density, cameras, points and edges in visibility graph are so many that the graph cut algorithm cannot work on one machine. To tackle this problem, we first divide the points just by KD-Tree [40] into the first-level blocks which can be split by graph cut and also collect all the cameras viewing those points in each first-level block to construct the sub-graphs. After that, we perform graph cut on each sub-graph to get the blocks which will be used in the distributed bundle adjustment algorithms. The details of the block splitting are listed below.

function SPLIT($\mathcal{E}$, $\mathcal{P}$, K, M) ▷ M is the maximum number of vertexes Normalized-Cut algorithm can deal with.
  Construct the visibility graph G where vertexes are cameras in $\mathcal{E}$ and points in $\mathcal{P}$ and there is an edge if one camera can view one point
  if $|\mathcal{E}| + |\mathcal{P}| \leq M$ **then**
    Split graph G by Normalized-Cut into K sub-graph and insert sub-graphs into $\mathcal{G}$
  else
    Split points into $K_s = (|\mathcal{E}| + |\mathcal{P}|)/M$ blocks by KD-Tree
    for each points block $B_i, i = 1, ..., K_s$ **do**
      Construct sub-graph $\widetilde{G}_i$ where vertexes are points in B_i and cameras viewing points in B_i
      Split graph $\widetilde{G}_i$ by Normalized-Cut into K/K_s sub-graph and insert sub-graphs into $\mathcal{G}$
    end for
  end if
  for each sub-graph $G_k \in \mathcal{G}$ **do**
    Insert all points in G_k into $\mathcal{P}_k$
    Insert all cameras in G with an edge to points in G_k into $\mathcal{E}_k$
  end for
end function

4.2 Parameter setting

Although we adopt the self-adaption scheme for the penalty parameters $\boldsymbol{\rho}$ in section 3.2, we still need set a proper initial value for the penalty parameters.

The analysis in section 3.1 shows that the penalty parameters should be larger than the Lipschitz constant of the objective function gradient. However, too large penalty parameters may lead to low convergence rate. The Lipschitz constant is difficult to estimate, so we set the initial penalty parameters intuitively according to the estimated range of parameters and the ratio of observations, cameras and points. Since the penalty parameters should balance the errors of $f(\mathcal{E}_k, \mathcal{D}_k, \mathcal{P}_k)$ and $h(\mathcal{E}_k, \mathcal{D}_k, \mathcal{P}_k)$ in Eqn. 14, the initial penalty parameters are set proportional to the ratio of observations, cameras and points as $\rho_x = \alpha_x|\mathcal{Q}|/N$ and $\rho_p = \alpha_p|\mathcal{Q}|/M$. ρ_x and α_x correspond to different kinds of camera parameters.

To unify the scale of input data, we first normalize the input SfM results so that the coordinates of camera centers are in $[-1,1]^3$. Then we set the penalty coefficient α_c on camera centers and α_p on points as 10^5. The angle-axis $\mathbf{r}_R$ of rotation are periodic and $\|\mathbf{r}_R - \mathbf{r}_R^0\| < 2\pi$, so it has the similar range to the normalized camera centers. Thus, the penalty coefficient α_r is also set as 10^5 for all cameras. The intrinsic parameters have their own ranges. In our experiment, we will optimize focal lengths, principle points and radial distortions simultaneously. Focal lengths and principle points are in the same order of magnitude as the image resolution and we set the penalty coefficient α_f and α_{uv} as 10^{-3}. Radial distortions are always less than 10^{-2}, we set the the penalty coefficient α_d on them as 10^4. The convergence threshold ϵ^{pri} and ϵ^{dual} in Eqn. 19 are set according to the initial penalty parameters. ϵ^{pri} is set as $10^{-5} \times N$ and ϵ^{dual} is set as $10^{-5} \times (2N\rho_r^0 + M\rho_p^0 + L(\rho_d^0 + 3\rho_f^0))$.

In the self-adaption scheme in section 3.2, we need to set four parameters μ_1, μ_2, τ^{incr} and τ^{decr}. Since the dual residuals are proportion with the penalty parameters and primal residuals are independent of the penalty parameters, generally, with large

This article has been accepted for publication in a future issue of this journal, but has not been fully edited. Content may change prior to final publication. Citation information: DOI 10.1109/TPAMI.2018.2840719, IEEE Transactions on Pattern Analysis and Machine Intelligence

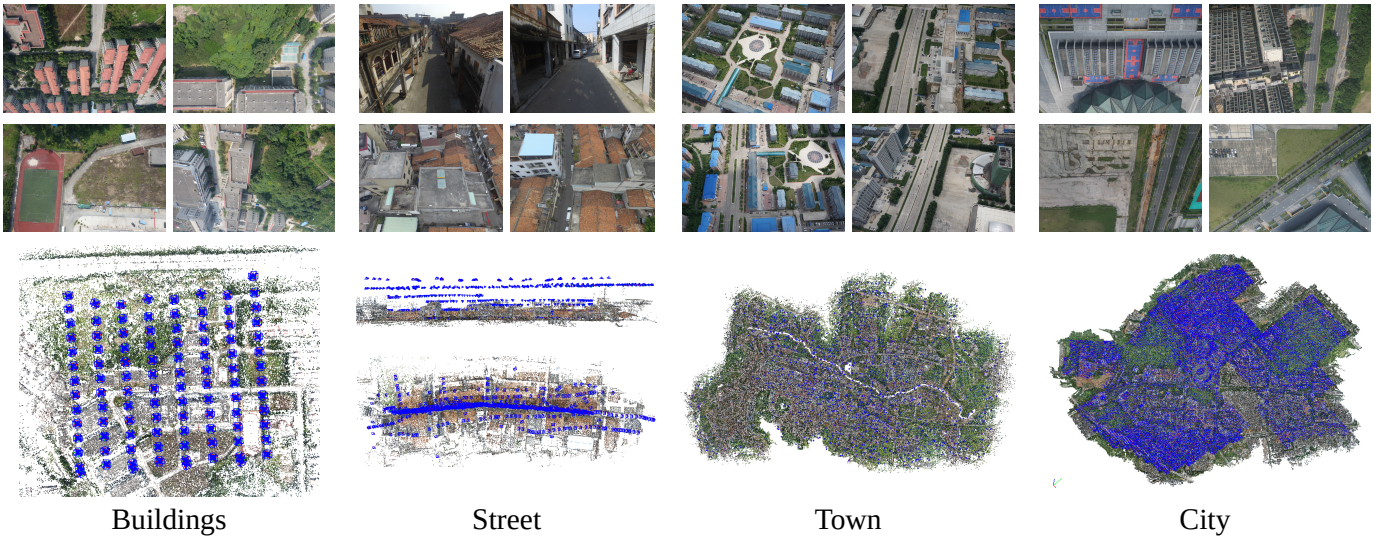

Fig. 2: Selected images and screenshots of the Structure-from-Motion results of **Buildings**, **Street**, **Town** and **City**. The first row is the selected images and the second row is the screenshots of SfM results, where the blue points are cameras. For **Street**, the top view and side view of SfM results are provided to show the data-set contains both aerial view and street view photos.

penalty parameters, the dual residuals are always much larger than the primal residuals in the iterations in Eqn. 26. Thus, we set μ according to the initial penalty parameters as $\mu_{1x} = 10/\rho_x^0$ and $\mu_{2x} = 10\rho_x^0$. τ^{incr} and τ^{decr} are both set as 2. In this way, the penalty parameters fluctuate on large enough values to guarantee the convergence. The over-relaxation coefficient in our experiments is set as 1.5.

5 Experimental Results

The proposed algorithm is implemented in C++ and run on PCs with Intel(R) Core(TM) i7-4770K 3.50GHz processors with 8 threads and 32GB memory. The communication speed is about 10MB/s among different nodes. We assign each thread one block and the number of used computers depends on the number of blocks according to the data scale. The method is a meta-algorithm independent of the specific optimization method for the iteration in Eqn. 14. Ceres Solver [41] with preconditioners in [19] is used as the optimization tool for each block's optimization in our experiments. We test our algorithm on the public online data-sets and our aerial photo data-sets. We choose the public online data-sets with number of images larger than 900 including **Roman Forum**, **Piccadilly**, **Trafalgar** [42], **Ladybug**, **Venice**, **Final 961** and **Final 13682** [16]. Our aerial photo data-sets include **Buildings**, **Street**, **Town** and **City** with high resolution 6000×4000 captured by DJI Phantom 4. **Buildings**, **Town** and **City** are captured in the aerial view and the cameras look towards the ground. **Street** is captured in both aerial and street view and some of cameras look forward in the street view. Selected images and screenshots of the Structure-from-Motion results of those four aerial photo data-sets are shown in Fig. 2. The number of intrinsic parameters shared by all cameras are one in **Buildings**, five in **Town** and 45 in **City**. Intrinsic parameters of cameras in other data-sets are independent. Since overlapping regions of the method of [21] for most of our data-sets account for at least half of the whole regions, it is nearly equivalent to do bundle adjustment in one machine. Therefore, we mainly compare our algorithm with the point consensus based method in [23]. To share intrinsic parameters in **Buildings**, **Town** and **City** in the experiment of the point consensus based method, we modify the method to average intrinsic parameters. Table 1 shows the numbers of cameras, points, observation, blocks of all data-sets and the optimized results by the traditional single machine bundle adjustment method [19] for above data-sets which can be optimized in one single machine.

5.1 Initialization

The local Lipschitz-continuity in section 3.1 requires the input of the optimization should be good enough, so the initialization, namely the Structure-from-Motion steps before the global bundle adjustment are very important.

We use a comprehensive Structure-from-Motion method [43] based on previous very large scale SfM works [7], [8], [44] with divide-and-conquer to obtain the SfM results before the final global bundle adjustment. In this method, the initial match graph of images is cut by a similar method with our splitting method in section 4.1, while the overlapping and completeness of each cluster are also guaranteed. Then local incremental SfM, which is implemented as Bundler [44], is performed in each cluster to register cameras in each cluster in each local coordinate system and filter out bad matches. At last, robust global motion averaging is performed on all clusters to register all cameras in a global coordinate system.

To guarantee the requirement in in section 3.1 that all depths are larger than d_{min} in the optimization, before the global bundle adjustment, we will filter outlier points according to their depths. We first compute the average depths of all points to all cameras. Then we filter out reprojections whose depths are less than 1% of the average depth.

In the following experiments, we first test how our splitting algorithm in section 4.1 optimizes the overhead and compare the overhead of our algorithm with the point consensus method [23]. Then, we compare the convergence of the two method. In the comparison, we will also show how the over-relaxation and self-adaption scheme affect the convergence rate.

This article has been accepted for publication in a future issue of this journal, but has not been fully edited. Content may change prior to final publication. Citation information: DOI 10.1109/TPAMI.2018.2840719, IEEE Transactions on Pattern Analysis and Machine Intelligence

TABLE 1: This table shows the data-scale of each data-set, containing the number of cameras(N), the number of points(M) and the number of observation($|\mathcal{Q}|$). K is the number of blocks, which is decided according to the number of cameras of each data-set. "Error" is the average reprojection error of each observation with unit pixel after the data is optimized by one single machine method implemented by Ceres Solver [41] with preconditioners in [19]. KDTree and NCut are different methods to split blocks for our algorithm. KDTree just splits blocks so that each block has the same number of points and NCut is the splitting algorithm described in section 4.1. PC is the point consensus method in [23]. Since [23] does not discuss the splitting method, we use the graph cut method similar to the method in section 4.1. N_c is the number of cameras to be broadcasted in one iteration in our algorithm and N_p is the number of points to be broadcasted in one iteration in method PC. B is the real size of data to be broadcasted in one iteration. T is the total time including computing and communication in one iteration. r_o is the ratio between the communication time and total time.

Dataset	N	M	$\|\mathcal{Q}\|$	K	Error	KDTree		NCut				PC			
						N_c	B(MB)	N_c	B(MB)	T(s)	r_o(%)	N_p	B(MB)	T(s)	r_o(%)
Buildings	510	260k	1.40M	32	1.21	5.12k	0.236	**4.57k**	**0.211**	**1.41**	**2.94**	190k	4.35	2.22	38.7
Final 961	961	187k	1.69M	32	0.760	26.4k	2.42	**25.4k**	**2.33**	**5.22**	**10.4**	155k	3.56	5.30	13.1
Roman Forum	1084	158k	1.12M	32	0.531	12.0k	1.10	**9.66k**	**0.884**	**7.16**	**2.89**	92.3k	2.11	7.18	4.61
Street	1130	347k	2.00M	64	1.04	22.6k	2.07	**13.6k**	**1.25**	**2.66**	**13.5**	156k	3.57	3.00	23.5
Ladybug	1723	157k	679k	64	0.739	19.9k	1.82	**10.2k**	**0.93**	**4.07**	**6.66**	66.9k	1.53	4.19	8.10
Venice	1778	994k	5.00M	64	1.11	21.6k	1.98	**20.6k**	**1.89**	**4.86**	**8.44**	352k	8.05	6.18	28.2
Piccadilly	2152	136k	9.20M	64	0.613	30.9k	2.83	**23.5k**	**2.15**	**8.89**	**5.61**	156k	3.56	9.06	9.63
Trafalgar	5288	214k	1.82M	128	-	92.7k	8.49	**53.4k**	**4.89**	**19.3**	**6.05**	354k	8.10	20.3	10.4
Final 13682	13682	4.46M	29.0M	256	-	511k	46.8	**282k**	**25.8**	**40.2**	**17.1**	4.65M	106	54.0	39.8
Town	36428	27.8M	3512M	1024	-	412k	18.9	**365k**	**17.3**	**22.8**	**12.2**	15.0M	342	105.6	80.0
City	138193	100.2M	10088M	2048	-	910k	45.9	**693k**	**35.9**	**73.1**	**10.5**	33.2M	760	167.4	70.9

5.2 Overhead

Fig. 4 shows the visualization of splitting results of each data-set. Since our splitting method divides the large problem by Normalized-Cut on camera graphs instead of regions, different blocks may intersect with each other, especially the results of **Final 961** and **Final 13682**. Since **City** is so large that the Normalized-Cut algorithms cannot work on it, KD-Tree [40] is performed first. The splitting result visualization of **City** in Fig. 4 shows the regular bounds of the KD-Tree splitting.

Table 1 shows the size of data to be broadcasted in one iteration, time used in one iteration and the ratio for which communication among different nodes accounts of total time in one iteration. Our method need broadcast all the camera parameters and each camera contains 6 extrinsic parameters and 6 camera intrinsic parameters according to our experiment configuration.

Firstly, we compare the splitting algorithm in section 4.1 with the method that just splits blocks equally by KD-Tree so that each block contains the same number of points. Table 1 demonstrates the splitting algorithm indeed reduces the total number of cameras to be broadcasted, especially for the densely captured data-set **Ladybug**, **Trafalgar**, **Final 13682** and **City**, for which the proposed method reduces nearly half of the data to be broadcasted.

Then, we compare the proposed method with the point consensus method in [23]. Since the splitting method is not discussed in [23], in the comparison, we modify the method in section 4.1 so that we collect the cameras and all the points viewed by those cameras after graph cut to minimize the points to be broadcasted in the point consensus method. Table 1 demonstrates that the cameras to be broadcasted in our method are less than the points to be broadcasted in the point consensus method by one or two orders of magnitude. Here, since we consider the optimization of camera intrinsic parameters in the bundle adjustment, each camera has to transfer 6 or 12 parameters, more than the parameters each point transfers. However, since the number of cameras to be broadcasted is much less than points, the total size of data to be broadcasted in our method is still less than the point consensus method. The more densely the data captured, the more data size reduced in broadcasting. On data-sets **Venice**, **Final 13682**, **Town** and **City**, the proposed method reduces the data to be broadcasted by 4 to 10 times in table 1.

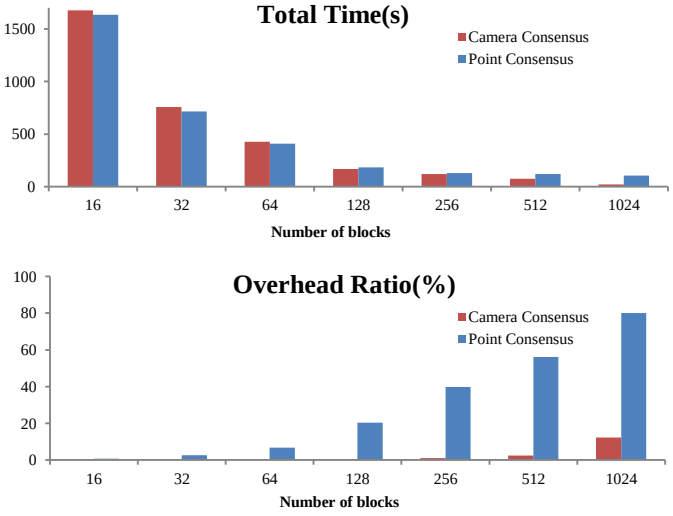

Fig. 3: The up is the total time of each iteration with different numbers of blocks. The down is the ratio of communication time and total time. The experiments are performed on **Town**.

Since our method splits blocks by points instead of cameras, the blocks in our methods have more cameras than points, while the blocks of points consensus method have more points than cameras. The number of cameras have more influence on the time used in local bundle adjustment of each block. Therefore, the local bundle adjustment of blocks in our method is a little slower than the compared method each iteration. However, with the increment of data scale and nodes used in the distributed system, the communication overhead accounts for more ratio among total time. Shown as Fig. 3, with the increment of number of used blocks, the total time reduces each iteration and the time cost by

This article has been accepted for publication in a future issue of this journal, but has not been fully edited. Content may change prior to final publication. Citation information: DOI 10.1109/TPAMI.2018.2840719, IEEE Transactions on Pattern Analysis and Machine Intelligence

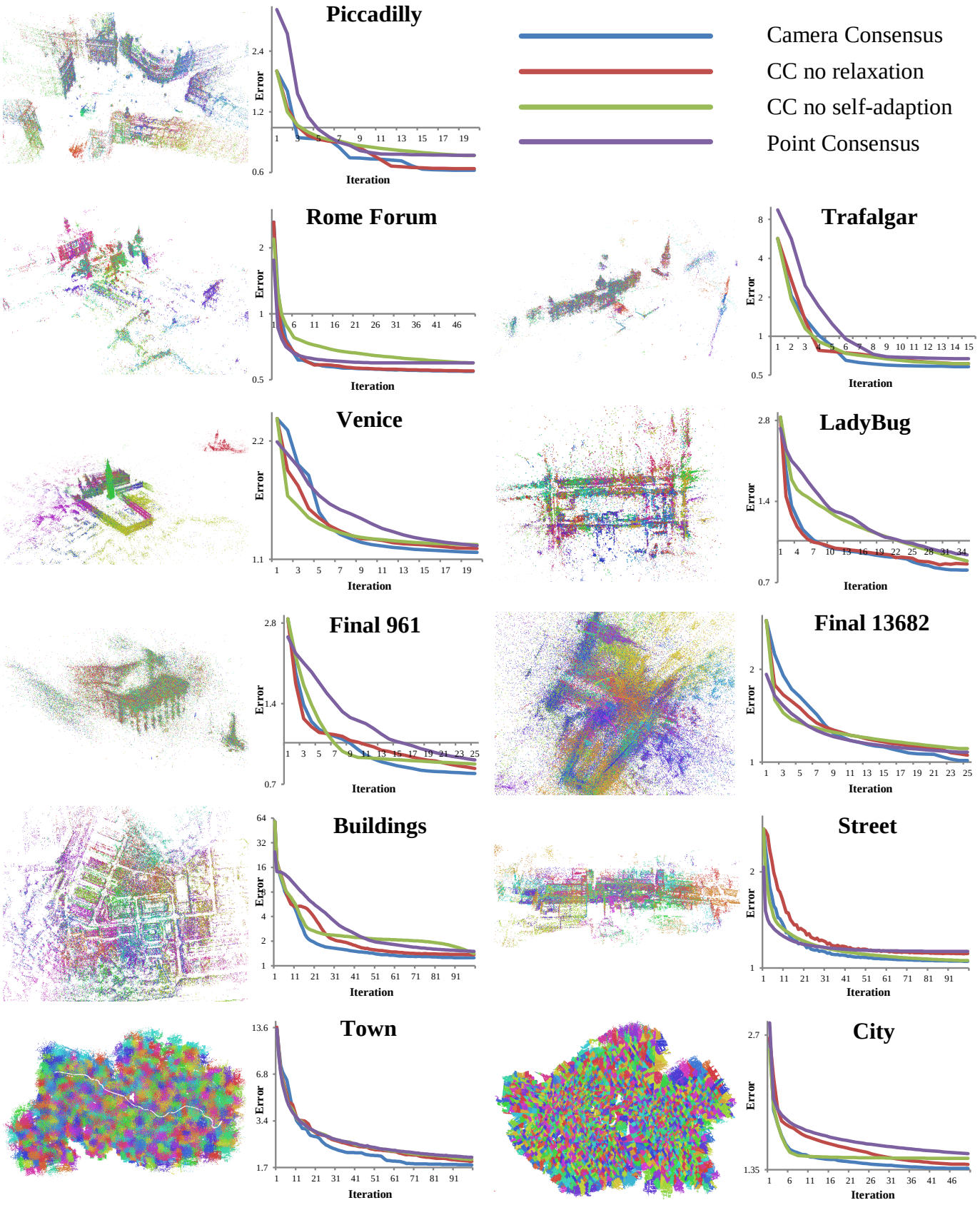

Fig. 4: The visualization of splitting results and convergence curves of each method for each data-set. In the visualization of splitting results, different colors mean differen blocks. The vertical axis of average reprojection errors uses the logarithmic scale to stand out the changes in the last iterations.

This article has been accepted for publication in a future issue of this journal, but has not been fully edited. Content may change prior to final publication. Citation information: DOI 10.1109/TPAMI.2018.2840719, IEEE Transactions on Pattern Analysis and Machine Intelligence

TABLE 2: This table shows the number of iterations when each method satisfies the stop criterion for each data-set and average reprojection errors of each observation when they converge. N_{it} is the number of iterations and "Error" is the average reprojection error of each observation with unit pixel. CC is our algorithm with over-relaxation and self-adaption scheme, which means camera consensus. CC_{nr} is our algorithm without the over-relaxation scheme and CC_{na} is the one without the self-adaption scheme. PC is the method in [23], meaning point consensus.

Dataset	Convergence							
	CC		CC_{nr}		CC_{na}		PC	
	N_{it}	Error	N_{it}	Error	N_{it}	Error	N_{it}	Error
Buildings	**64**	**1.23**	72	1.35	100	1.39	87	1.43
Final 961	22	**0.763**	30	0.801	**14**	0.820	25	0.864
Roman Forum	**22**	**0.536**	25	0.542	50	0.590	23	0.597
Street	85	**1.04**	87	1.10	100	1.05	**76**	1.08
Ladybug	**31**	**0.745**	32	0.801	34	0.810	32	0.837
Venice	16	**1.13**	17	1.15	**12**	1.18	20	1.17
Piccadilly	17	**0.614**	13	0.625	19	0.686	**11**	0.688
Trafalgar	**10**	**0.580**	15	0.601	12	0.597	**10**	0.619
Final 13682	24	**1.01**	30	1.04	23	1.08	**22**	1.07
Town	**83**	**1.76**	96	1.87	98	1.89	96	1.91
City	41	**1.36**	59	1.38	**34**	1.43	61	1.41

communication increases. The communication time in our method increases much slower than the compared method. For **Town** in Fig. 3, the total cost time each iteration in our method is less than the compared method after the number of blocks is larger than 128. On large scale data-sets **Final 13682**, **Town** and **City**, our method saves 20%-80% time, while the point consensus method spends more than half of time on communication. Therefore, our method has higher scalability when we use more blocks and deal with larger scale data-sets.

5.3 Convergence

Fig. 4 shows the convergence curves of each method for each data-set and table 2 provides the average reprojection error of each observation and the number of iteration when the algorithms satisfy the stop criterion in Eqn. 19.

We first test the over-relaxation and self-adaption scheme for our algorithm. The curve in Fig. 4 shows that the over-relaxation facilitates the convergence after several iterations. To test the effect of the self-adaption scheme, we adopt the strategy in [23] for the algorithm without self-adaption as comparison. In that strategy, the penalty parameters increase 0.01 times in each iteration. Table 2 shows that the algorithm without self-adaption converges slowly or converges fast in a larger error. Fig. 4 shows that the algorithm with self-adaption always has a non-smooth curve. The reason is the penalty parameters decrease when the primary residual is much smaller than the dual residual and the curve will converge faster after the penalty is set smaller.

To compare with the point consensus method in [23], we modify the penalty parameter setting in [23] since we normalize all the data-sets. The initial penalty parameter on each point position is $10^5 \times |\mathcal{Q}|/M$ same as the one in our method. We also adopt the over-relaxation and the self-adaption scheme on the point consensus method. Table 2 shows the point consensus method always converges in little larger errors, though it converges faster for some data-sets. Intuitively, single points influence weaker than cameras in the bundle adjustment problem and the more parameters to be averaged, the slower the ADMM algorithm converges. Thus, camera consensus method outperforms the point consensus one on convergence rate.

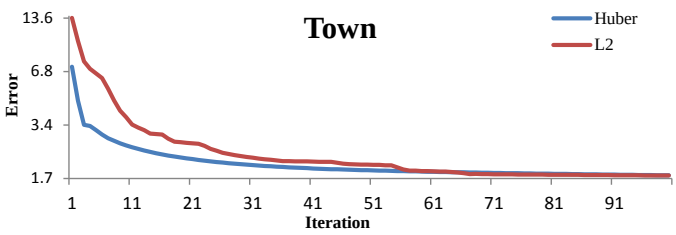

Fig. 5: Convergence curves of L2-normal and Huber loss on data-set **Town**. The vertical axis of average loss per reprojection uses the logarithmic scale to stand out the changes in the last iterations.

6 Discussion

In this section, we will discuss some problems in our practical large scale projects and the future work.

6.1 Robust loss function

In section 3.1, we obtain the conclusion that the proposed method requires the gradient of the objective function should be local Lipschitz-continuous. Therefore, if one robust loss function does not break Lipschitz-continuity of the objective function gradients, the robust loss function can be used here to replace the $l2$ normal loss.

Here, we try to use one commonly used robust loss function - Huber loss [45] in our practical projects. In Huber loss, the loss will be linear with the error when the error exceeds the threshold, otherwise it is the square of errors. Since the gradient of the linear interval is much smaller than the square one, it has smaller local Lipschitz-constants. The analysis in section 3.1 shows that penalty parameters ρ should be larger than the lipschitz-constant, so Huber loss requires smaller penalty parameters and may accelerate the convergence rate. Here, we show the comparison of convergence curves obtained by our method with $l2$ normal and Huber loss in Fig. 5. This experiment is performed on data-set **Town**. The threshold parameter of Huber loss is set as 4 here. Since Huber loss objective function has lower loss than L2-normal, the average loss is smaller. Fig. 5 shows Huber loss objective function converges faster.

6.2 Post-optimization

Although we set a stopping criterion in Eqn. 19, sometimes, the practical large projects do not reach the criterion after many iterations. Therefore, in practice, we also set a maximum iteration number to stop the method to guarantee the global bundle adjustment can be completed in required time. However, if the method is not stopped by the stopping criterion in Eqn. 19, the cameras will not be accurate enough for the following 3D reconstruction steps, since the camera poses are just averaged in the end. To guarantee the camera accuracy for the following 3D reconstruction steps, we will fix all points and optimize each camera or each camera group in parallel. Since the bundle adjustment of each camera or camera group requires much smaller memory and can be performed in parallel, this step is scalable and fast. Since the points have been optimized to good enough positions in previous ADMM iterations, the cameras poses by this pose-optimization are accurate enough.

6.3 Outlier cameras

The convergence condition local Lipschitz-continuity in section 3.1 actually requires we have a good enough initialization and all the depths should be larger than d_{min} in the optimization process. However, in practice, the previous Structure-from-Motion steps may pass some outlier cameras which have many mismatches and should have been filtered out. We find that, in the ADMM iterations, these outlier cameras always introduce large reprojection errors and those outlier reprojections always have small depths, which means that the requirement in section 3.1 is not satisfied. In the following iterations, one outlier camera with large reprojection errors will propagate its wrong poses to its neighborhood in the next iteration and result the whole data-set into divergency.

To avoid this situation, in each iteration, we should check the reprojection errors of each camera. If we find one camera have a very large reprojection error, we should remove this camera immediately before its error propagates to others. After outlier cameras are removed, the energy function will tend to descend stably instead of divergency. This remedy forces all the variables satisfy the requirement in section 3.1 in the optimization process.

6.4 Future work

As [25] says, ADMM algorithm may be very slow to converge compared with traditional optimization methods, such as Newton's method or LM algorithm. Therefore, we suggest the proposed method should be used in very large scale data-sets, especially in the case that in-core optimization methods cannot work. In small data-sets, the proposed method may be slower than in-core methods since it may need many iterations of in-core methods to converge though each iteration is fast. Therefore, we may try ADMM algorithm on other very large scale 3D reconstruction tasks.

One of large scale 3D reconstruction tasks that ADMM algorithm can work on is global motion averaging in Structure-from-Motion. In the divide-and-conquer SfM method [43], although incremental SfM of each small block can be completed in parallel to decompose the large scale problem, the method requires global motion averaging to register all the small blocks into a global coordinate system. The global motion averaging task has the similar space cost with the global bundle adjustment, but it also has its own difficulties. One reason why ADMM algorithm can work on the non-convex problem bundle adjustment is that we already has good enough initialization before the global bundle adjustment. However, in the global motion averaging task, we do not have an initialization and rotation averaging task is non-convex. Some translation averaging objective functions [46], [47] are convex and ADMM algorithm can be applied on them. Another problem is the topology of tasks. The reason why the bundle adjustment problem can be decomposed easily is that the problem is defined on a bipartite graph, camera-points visibility graph. But motion averaging tasks are always defined on camera connection graph, it is not easy to define the variables to be consensus. We should also consider above problems when we want to apply ADMM algorithms to other optimization tasks in 3D reconstruction.

7 Conclusion

In this paper, we propose a distributed bundle adjustment algorithm based on camera consensus for very large scale data-sets. Our key contribution is that we distribute points in different nodes of the distributed system and broadcast cameras for consensus. The camera consensus reduces the size of data to be broadcasted in each iteration and thus saves much overhead in the distributed system. Besides, we adopt the over-relaxation and self-adaption scheme to improve the convergence rate. The experiments demonstrate our camera consensus method outperforms the state-of-the-art method in efficiency and accuracy. In the end, we discuss some problems which should be noted in practice and other 3D reconstruction tasks which ADMM algorithms can work on.

Acknowledgments

This work is supported by Hong Kong RGC 16208614, T22-603/15N, Hong Kong ITC PSKL12EG02, and China 973 program, 2012CB316300.

References

[1] S. Zhu, T. Fang, J. Xiao, and L. Quan, "Local readjustment for high-resolution 3d reconstruction," in *The IEEE Conference on Computer Vision and Pattern Recognition (CVPR)*, June 2014.

[2] R. Zhang, S. Li, T. Fang, S. Zhu, and L. Quan, "Joint camera clustering and surface segmentation for large-scale multi-view stereo," in *The IEEE International Conference on Computer Vision (ICCV)*, December 2015.

[3] D. P. Bertsekas and J. N. Tsitsiklis, *Parallel and distributed computation: numerical methods*. Prentice hall Englewood Cliffs, NJ, 1989, vol. 23.

[4] M. Lhuillier and L. Quan, "A quasi-dense approach to surface reconstruction from uncalibrated images," *Pattern Analysis and Machine Intelligence, IEEE Transactions on*, vol. 27, no. 3, pp. 418–433, 2005.

[5] N. Snavely, S. M. Seitz, and R. Szeliski, "Modeling the world from internet photo collections," *International Journal of Computer Vision*, vol. 80, no. 2, pp. 189–210, 2008.

[6] T. Fang and L. Quan, "Resampling structure from motion," *Computer Vision–ECCV 2010*, pp. 1–14, 2010.

[7] S. Agarwal, Y. Furukawa, N. Snavely, I. Simon, B. Curless, S. M. Seitz, and R. Szeliski, "Building rome in a day," *Communications of the ACM*, vol. 54, no. 10, pp. 105–112, 2011.

[8] N. Snavely, S. M. Seitz, and R. Szeliski, "Skeletal graphs for efficient structure from motion," in *The IEEE Conference on Computer Vision and Pattern Recognition (CVPR)*, June 2008.

[9] J.-M. Frahm, P. Fite-Georgel, D. Gallup, T. Johnson, R. Raguram, C. Wu, Y.-H. Jen, E. Dunn, B. Clipp, S. Lazebnik *et al.*, "Building rome on a cloudless day," in *European Conference on Computer Vision*. Springer, 2010, pp. 368–381.

[10] J. Heinly, J. L. Schonberger, E. Dunn, and J.-M. Frahm, "Reconstructing the world* in six days *(as captured by the yahoo 100 million image dataset)," in *The IEEE Conference on Computer Vision and Pattern Recognition (CVPR)*, June 2015.

[11] B. Klingner, D. Martin, and J. Roseborough, "Street view motion-from-structure-from-motion," in *The IEEE International Conference on Computer Vision (ICCV)*, December 2013.

[12] J. L. Schonberger, F. Radenovic, O. Chum, and J.-M. Frahm, "From single image query to detailed 3d reconstruction," in *The IEEE Conference on Computer Vision and Pattern Recognition (CVPR)*, June 2015.

[13] T. Shen, S. Zhu, T. Fang, R. Zhang, and L. Quan, "Graph-based consistent matching for structure-from-motion," in *European Conference on Computer Vision*. Springer, 2016, pp. 139–155.

[14] J. L. Schonberger and J.-M. Frahm, "Structure-from-motion revisited," in *The IEEE Conference on Computer Vision and Pattern Recognition (CVPR)*, June 2016.

[15] B. Triggs, P. F. McLauchlan, R. I. Hartley, and A. W. Fitzgibbon, "Bundle adjustmentła modern synthesis," in *Vision algorithms: theory and practice*. Springer, 2000, pp. 298–372.

[16] S. Agarwal, N. Snavely, S. M. Seitz, and R. Szeliski, "Bundle adjustment in the large," in *European Conference on Computer Vision*. Springer, 2010, pp. 29–42.

[17] L. Carlone, P. Fernandez Alcantarilla, H.-P. Chiu, Z. Kira, and F. Dellaert, "Mining structure fragments for smart bundle adjustment," in *Proceedings of the British Machine Vision Conference*. BMVA Press, 2014.

[18] Y.-D. Jian, D. C. Balcan, and F. Dellaert, "Generalized subgraph preconditioners for large-scale bundle adjustment," in *Outdoor and Large-Scale Real-World Scene Analysis*. Springer, 2012, pp. 131–150.

[19] A. Kushal and S. Agarwal, "Visibility based preconditioning for bundle adjustment," in *The IEEE Conference on Computer Vision and Pattern Recognition (CVPR)*, June 2012.

[20] C. Wu, S. Agarwal, B. Curless, and S. M. Seitz, "Multicore bundle adjustment," in *The IEEE Conference on Computer Vision and Pattern Recognition (CVPR)*, June 2011.

[21] K. Ni, D. Steedly, and F. Dellaert, "Out-of-core bundle adjustment for large-scale 3d reconstruction," in *Proceedings of the IEEE International Conference on Computer Vision*, 2007, pp. 1–8.

[22] K. Ni and F. Dellaert, "Hypersfm," in *2012 Second International Conference on 3D Imaging, Modeling, Processing, Visualization & Transmission*. IEEE, 2012, pp. 144–151.

[23] A. Eriksson, J. Bastian, T.-J. Chin, and M. Isaksson, "A consensus-based framework for distributed bundle adjustment," in *The IEEE Conference on Computer Vision and Pattern Recognition (CVPR)*, June 2016.

[24] F. Dellaert and M. Kaess, "Square root sam: Simultaneous localization and mapping via square root information smoothing," *The International Journal of Robotics Research*, vol. 25, no. 12, pp. 1181–1203, 2006.

[25] S. Boyd, N. Parikh, E. Chu, B. Peleato, and J. Eckstein, "Distributed optimization and statistical learning via the alternating direction method of multipliers," *Foundations and Trends® in Machine Learning*, vol. 3, no. 1, pp. 1–122, 2011.

[26] M. Fukushima and H. Mine, "A generalized proximal point algorithm for certain non-convex minimization problems," *International Journal of Systems Science*, vol. 12, no. 8, pp. 989–1000, 1981.

[27] A. Kaplan and R. Tichatschke, "Proximal point methods and nonconvex optimization," *Journal of global Optimization*, vol. 13, no. 4, pp. 389–406, 1998.

[28] S. Sra, "Scalable nonconvex inexact proximal splitting," in *Advances in Neural Information Processing Systems*, 2012, pp. 530–538.

[29] G. Li and T. K. Pong, "Global convergence of splitting methods for nonconvex composite optimization," *SIAM Journal on Optimization*, vol. 25, no. 4, pp. 2434–2460, 2015.

[30] M. Hong, Z.-Q. Luo, and M. Razaviyayn, "Convergence analysis of alternating direction method of multipliers for a family of nonconvex problems," *SIAM Journal on Optimization*, vol. 26, no. 1, pp. 337–364, 2016.

[31] L. Yang, T. K. Pong, and X. Chen, "Alternating direction method of multipliers for a class of nonconvex and nonsmooth problems with applications to background/foreground extraction," *SIAM Journal on Imaging Sciences*, vol. 10, no. 1, pp. 74–110, 2017.

[32] C. Olsson, F. Kahl, and R. Hartley, "Projective least-squares: Global solutions with local optimization," in *The IEEE Conference on Computer Vision and Pattern Recognition (CVPR)*, June 2009.

[33] G. Gallego and A. Yezzi, "A compact formula for the derivative of a 3-d rotation in exponential coordinates," *Journal of Mathematical Imaging and Vision*, vol. 51, no. 3, pp. 378–384, Mar 2015. [Online]. Available: https://doi.org/10.1007/s10851-014-0528-x

[34] B. He, H. Yang, and S. Wang, "Alternating direction method with self-adaptive penalty parameters for monotone variational inequalities," *Journal of Optimization Theory and applications*, vol. 106, no. 2, pp. 337–356, 2000.

[35] J. Eckstein and D. P. Bertsekas, "On the douglas-rachford splitting method and the proximal point algorithm for maximal monotone operators," *Mathematical Programming*, vol. 55, no. 1-3, pp. 293–318, 1992.

[36] H. H. Bauschke, P. L. Combettes *et al.*, *Convex analysis and monotone operator theory in Hilbert spaces*. Springer, 2017, vol. 2011.

[37] J. Eckstein, "Parallel alternating direction multiplier decomposition of convex programs," *Journal of Optimization Theory and Applications*, vol. 80, no. 1, pp. 39–62, 1994.

[38] J. Eckstein and M. C. Ferris, "Operator-splitting methods for monotone affine variational inequalities, with a parallel application to optimal control," *INFORMS Journal on Computing*, vol. 10, no. 2, pp. 218–235, 1998.

[39] J. Shi and J. Malik, "Normalized cuts and image segmentation," *Pattern Analysis and Machine Intelligence, IEEE Transactions on*, vol. 22, no. 8, pp. 888–905, 2000.

[40] J. L. Bentley, "Multidimensional binary search trees used for associative searching," *Communications of the ACM*, vol. 18, no. 9, pp. 509–517, 1975.

[41] S. Agarwal, K. Mierle, and Others, "Ceres solver," http://ceres-solver.org.

[42] K. Wilson and N. Snavely, "Robust global translations with 1dsfm," in *European Conference on Computer Vision*. Springer, 2014, pp. 61–75.

[43] S. Zhu, T. Shen, L. Zhou, R. Zhang, T. Fang, and L. Quan, "Accurate, scalable and parallel structure from motion," *CoRR*, vol. abs/1702.08601, 2017. [Online]. Available: http://arxiv.org/abs/1702.08601

[44] N. Snavely, S. M. Seitz, and R. Szeliski, "Photo tourism: exploring photo collections in 3d," in *ACM transactions on graphics*, vol. 25, no. 3. ACM, 2006, pp. 835–846.

[45] P. J. Huber *et al.*, "Robust estimation of a location parameter," *The Annals of Mathematical Statistics*, vol. 35, no. 1, pp. 73–101, 1964.

[46] N. Jiang, Z. Cui, and P. Tan, "A global linear method for camera pose registration," in *The IEEE International Conference on Computer Vision (ICCV)*, December 2013.

[47] Z. Cui and P. Tan, "Global structure-from-motion by similarity averaging," in *The IEEE International Conference on Computer Vision (ICCV)*, December 2015.

Runze Zhang is currently a PhD Candidate advised by Professor Long Quan in the Department of Computer Science and Engineering, the Hong Kong University of Science and Technology. He received the bachelor degree in intelligence science and technology from Peking University, China. His research interests include computer vision and computer graphics, especially large-scale 3D reconstruction.

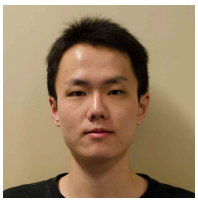

Siyu Zhu received the bachelor degree in computer science from Zhejiang University, China, in 2012, and PhD degree in computer science from the Hong Kong University of Science and Engineering in 2017. He is currently a senior algorithm engineer in Alibaba A.I. Labs. His research interests include computer vision and computer graphics, especially large-scale 3D reconstruction.

Tianwei Shen is a Ph.D. candidate in the Department of Computer Science and Engineering, Hong Kong University of Science and Technology, advised by Professor Long Quan. Previously, He obtained the bachelor degree from Peking University, double major in machine intelligence (EECS) and psychology. His research focuses on large-scale 3D reconstruction and geometric learning problems in 3D vision.

Lei Zhou is a PhD candidate in the Department of Computer Science and Engineering, HKUST from 2015. Prior to this, he received bachelor's degree in information science and electronic engineering from Zhejiang University, China, in 2015. His research interests include image matching, structure from motion, SLAM and 3D reconstruction.

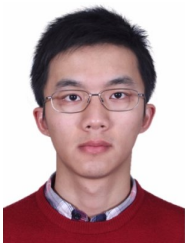

Zixin Luo received his bachelor degree in Department of Automation at Tsinghua University in Beijing, China. He is now a PhD student at Hong Kong University of Science and Technology under the supervision of Prof. Long Quan. His research interests include matching tasks in 3D computer vision.

Tian Fang received the bachelor and master degree in Computer Science and Engineering from the South China University of Technology, China, in 2003 and 2006, respectively, and received the Ph.D. degree in Computer Science and Engineering from the Hong Kong University of Science and Technology (HKUST) in 2011. He was a research assistant professor in HKUST from 2014 to 2016. His research interests include large scale image-based modeling, mesh vectorization, image segmentation, recognition, and photo-realistic rendering. He co-founded Altizure.com, a realistic 3D modeling platform providing internet solutions for 3D reconstruction and online 3D application.

Long Quan received the Ph.D. in Computer Science at INRIA, France, in 1989. He is now a professor of the Department of Computer Science and Engineering at the Hong Kong University of Science and Technology. He is an IEEE Fellow of the Computer Society. He has served in all the major computer vision journals, as an Associate Editor of IEEE Transactions on Pattern Analysis and Machine Intelligence (PAMI), a Regional Editor of Image and Vision Computing Journal (IVC), an editorial board member of the International Journal of Computer Vision (IJCV), an editorial board member of the Electronic Letters on Computer Vision and Image Analysis (ELCVIA), an associate editor of Machine Vision and Applications (MVA), and an editorial member of Foundations and Trends in Computer Graphics and Vision.